

Turbulence and droplets in clouds & in the laboratory with emphasis on the effects of initial and boundary conditions: Gravitational effects in flows with inertial particles.

1. Cloud and laboratory parameters
2. Entrainment experiments with inertial particles
3. Boundary layer experiments with inertial particles
4. DNS of boundary layer with inertial particles*



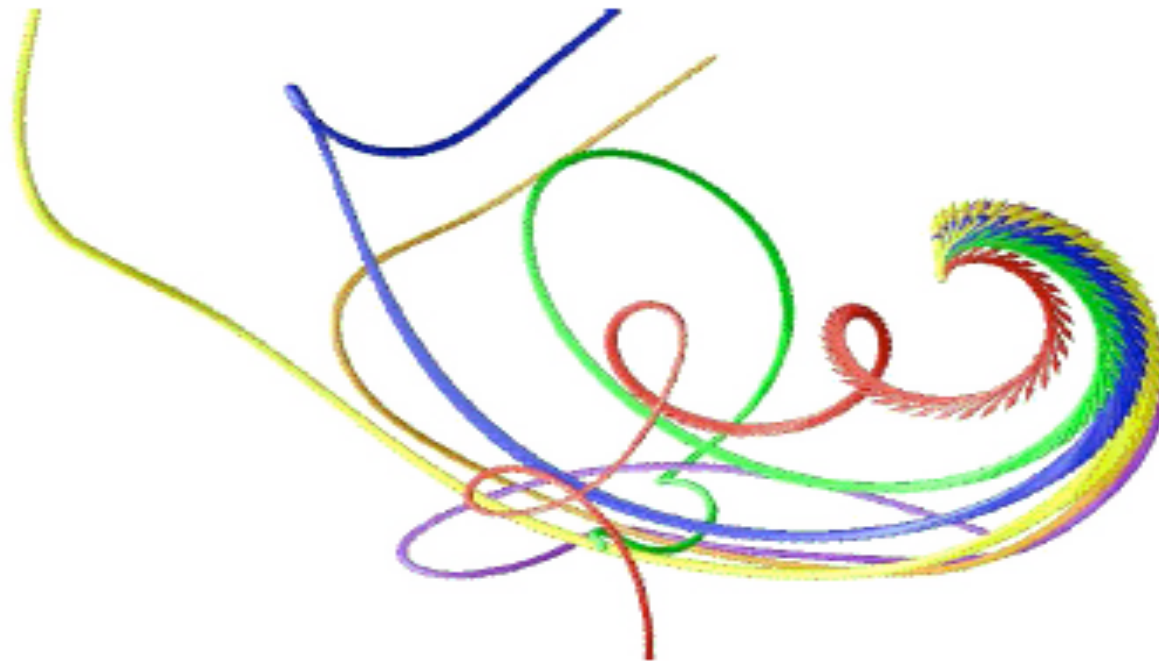
Experiments with Sergiy Geraschenko and Garrett Good, Cornell University.

*DNS with Valentina Lavezzo, Alfredo Soldati & Lance Collins

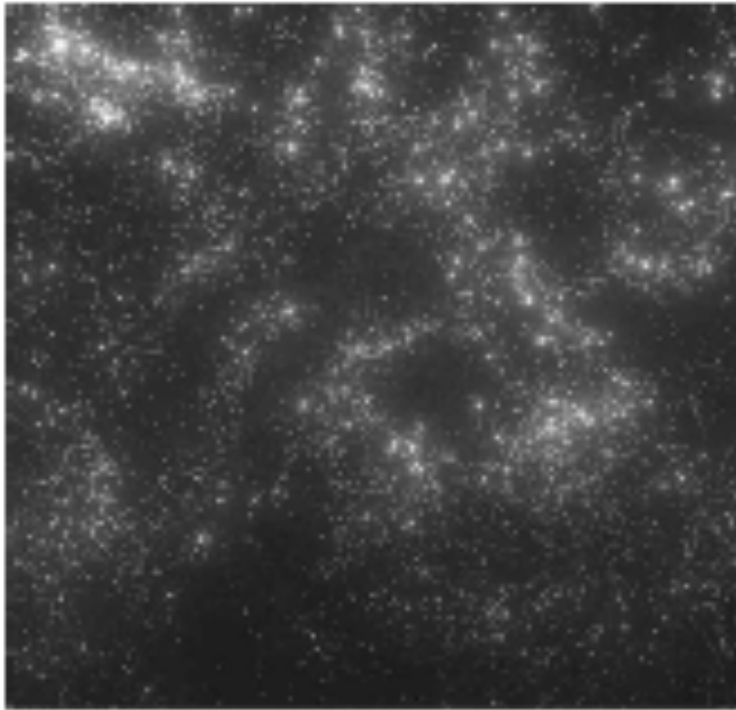
INERTIAL PARTICLES:

Preferential sampling: Red:tracer,
Green,blue,brown,yellow, increasing inertial effects

Toschi and Bodenschatz, 2009. (DNS)

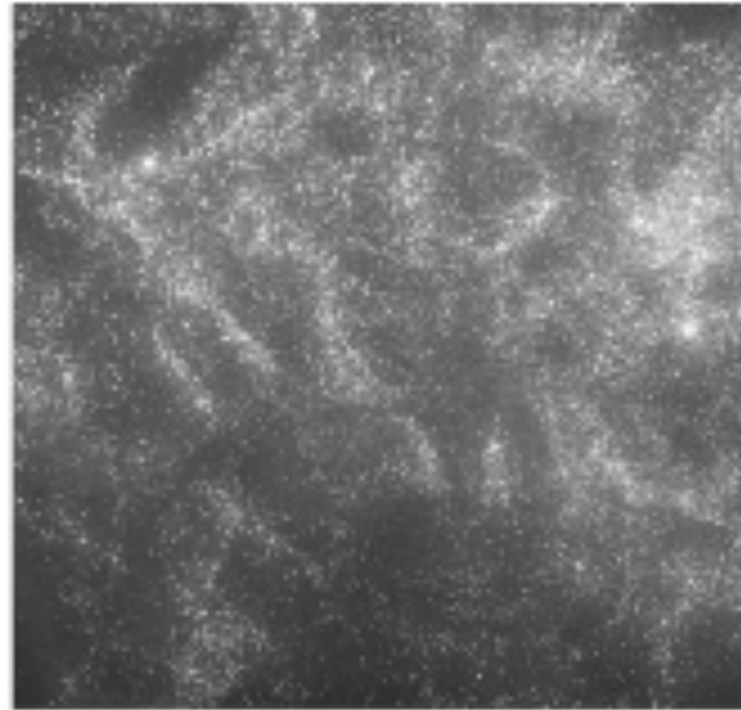


Experiments on inertial particle clustering : Wood, Hwang & Eaton. 2005



(a)

$St=0.57$



(b)

$St=1.33$

Maxey and Corrsin (1986), Wang and Maxey (1993),
Davila & Hunt (2001).....

54

L.-P. Wang and M. R. Maxey

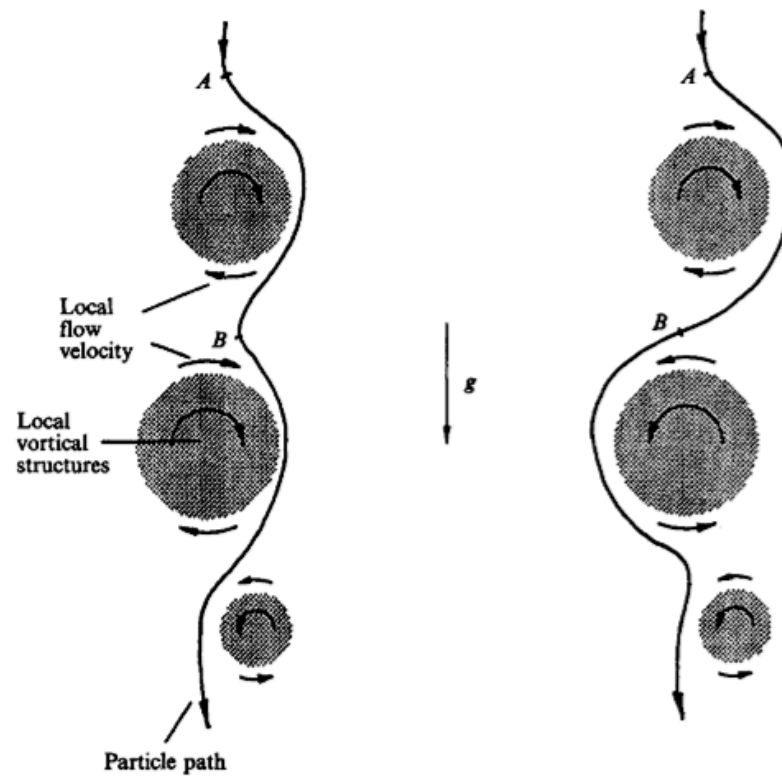
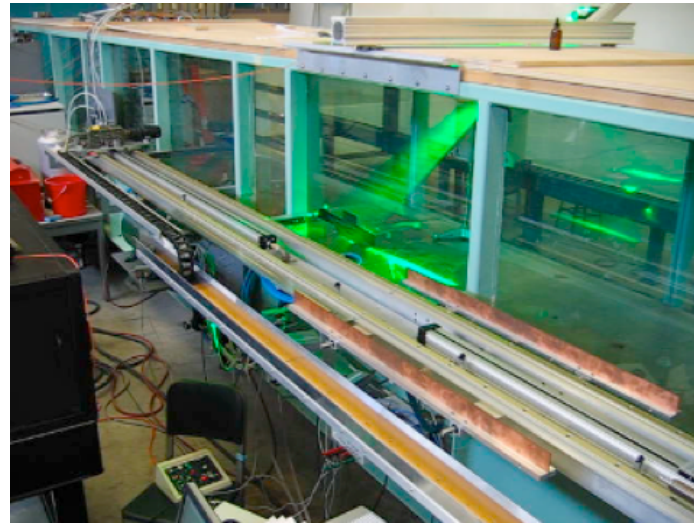


FIGURE 13. Sketch showing the preferential sweeping mechanism for a heavy particle interacting with local flow vortical structures under its inertia and body force.

1. CLOUD & LABORATORY PARAMETERS



Parameters:

- Reynolds number

$$R_\lambda = \frac{u\lambda}{\nu}$$

- Stokes number ---- (Particle relaxation time/Kolmogorov time scale).

$$St \equiv \frac{\tau_p}{\tau_\eta} = \frac{\beta d^2 / 18\nu}{(\nu/\varepsilon)^{1/2}}, \quad \beta = \frac{\rho_p}{\rho}$$

$$st \sim d^2 \varepsilon^{1/2}$$

- Froude number

$$Fr_{inertial} = gSt / \langle a^2 \rangle^{1/2}$$

- -Ratio of terminal velocity to Kolmogorov velocity

$$v_g / v_\eta \sim d^2 \varepsilon^{-1/4}$$

Particle diameter /Kolmogorov Scale

$$d / \eta$$

Siebert et al. Atmospheric Research 2010

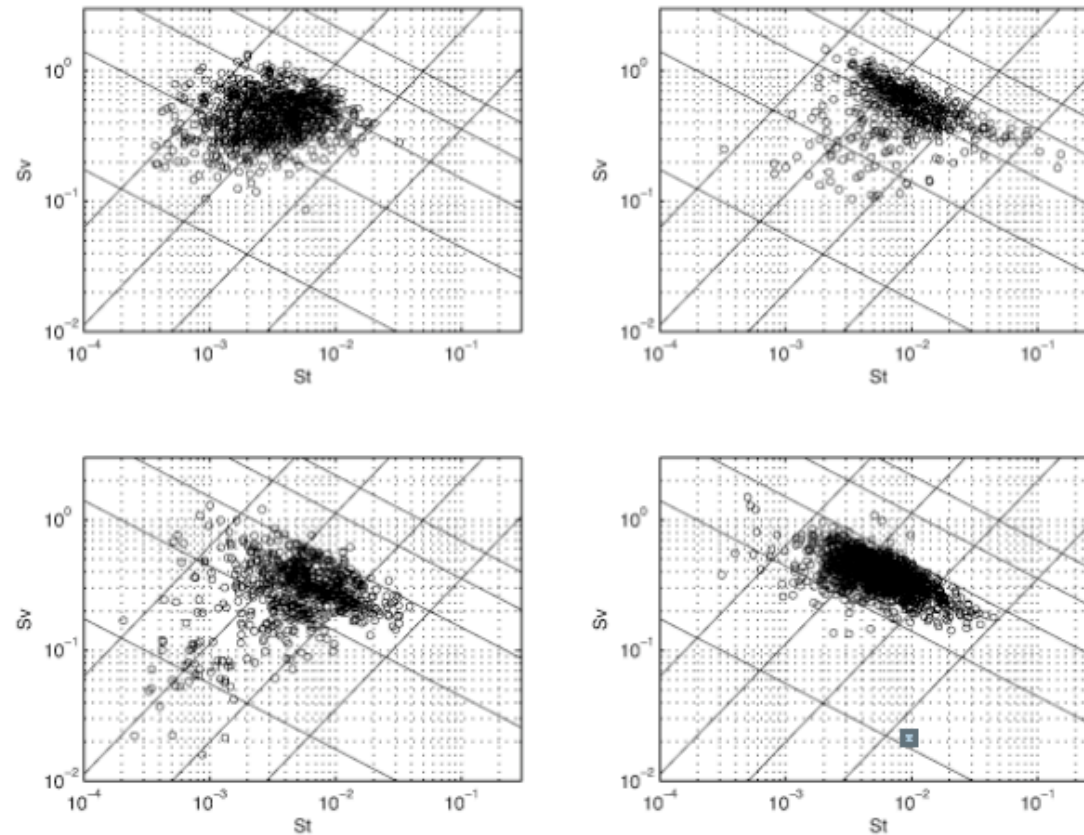


Figure 9: The distribution of cloud microphysical and turbulence properties in a dimensionless Stokes–settling parameter space. The upper left plot is for a stratocumulus cloud and the remaining three are for small cumulus clouds. Each point represents data in a 1-second (approximately 15 meter) average. Diagonal lines with positive slope are contours of constant turbulent energy dissipation rate, ε , at values of 10^{-4} , 10^{-3} , 10^{-2} , and 10^{-1} (lower right to upper left corners). Diagonal lines with negative slope are contours of constant droplet diameter at values of 5, 10, 15, 20 and $25 \mu\text{m}$ (lower left to upper right corners).

Parameter ranges in clouds and in the laboratory

Cornell droplet experiments:

$$Re_\lambda = 275, St = 0.2, Sv = 0.37, Fr = 0.54 \text{ and } \epsilon = 0.1 m^2/s^3$$

Cumuluous clouds (Seibert, Shaw et al.)

$$Re_\lambda \text{ is in the range } 10^3 - 10^4, St \sim 10^{-3} - 10^{-1}, Sv \sim 10^{-2} - 10^0, \epsilon \sim 10^{-4} - 10^{-1}$$

Seibert, Shaw et al. JAS 2010

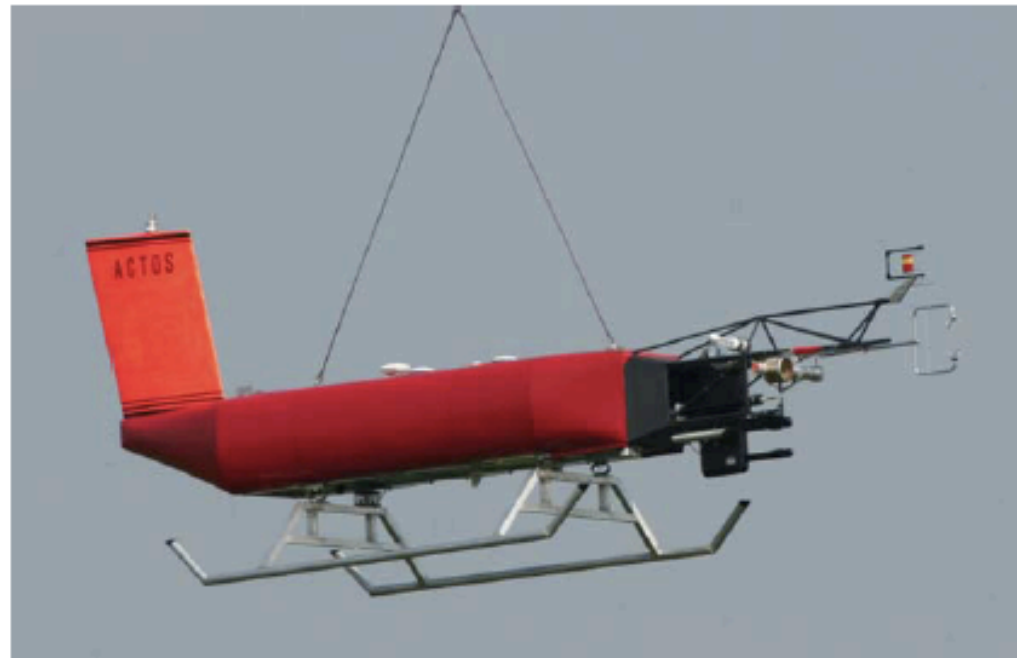


Figure 1: ACTOS comprises instrumentation for comprehensive measurements of thermodynamic, microphysical, and turbulent variables in clouds, at high spatial resolution. The ACTOS measurement payload is attached to the helicopter by means of a 140 m long tether cable. The true airspeed of the helicopter is about 15 m/s, sufficient to enable stable flight conditions of ACTOS out of the helicopter's downwash.

Velocity statistics in a stratocumulus cloud.

Seibert et. al JAS 2010, Atmos. Res. 2010

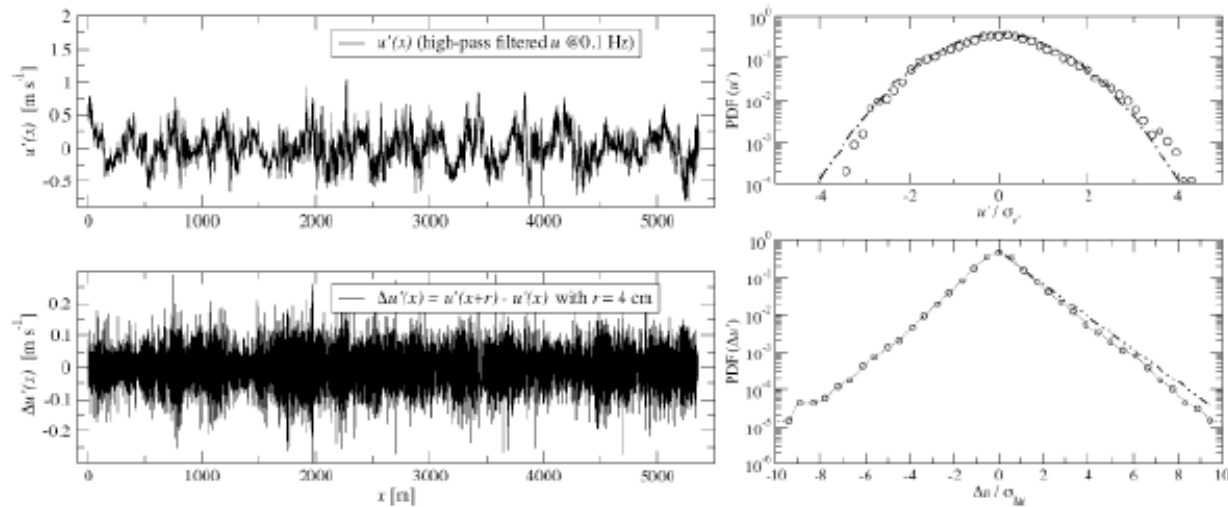


Figure 4: Left panel: Time series of velocity fluctuations $u'(x)$ (upper panel) and increments $\Delta u'(x) = u'(x+r) - u'(x)$ (with fixed $r = 4$ cm) (lower panel) derived from despiked hot-wire data in a stratocumulus field. The fluctuations u' are calculated by applying a high-pass filter (2nd-order Butterworth filter) with a cut-off frequency of 0.1 Hz corresponding to a wavelength of 150 m. Right panel: Probability density functions (PDFs) of u' (upper panel) and $\Delta u'$ (lower panel). A Gaussian fit of $p(u')$ and an exponential fit of the tails of $p(\Delta u')$ are included as reference. From Siebert et al. (2010). Copyright 2010, American Meteorological Society.

Seibert et al. JAS 2010

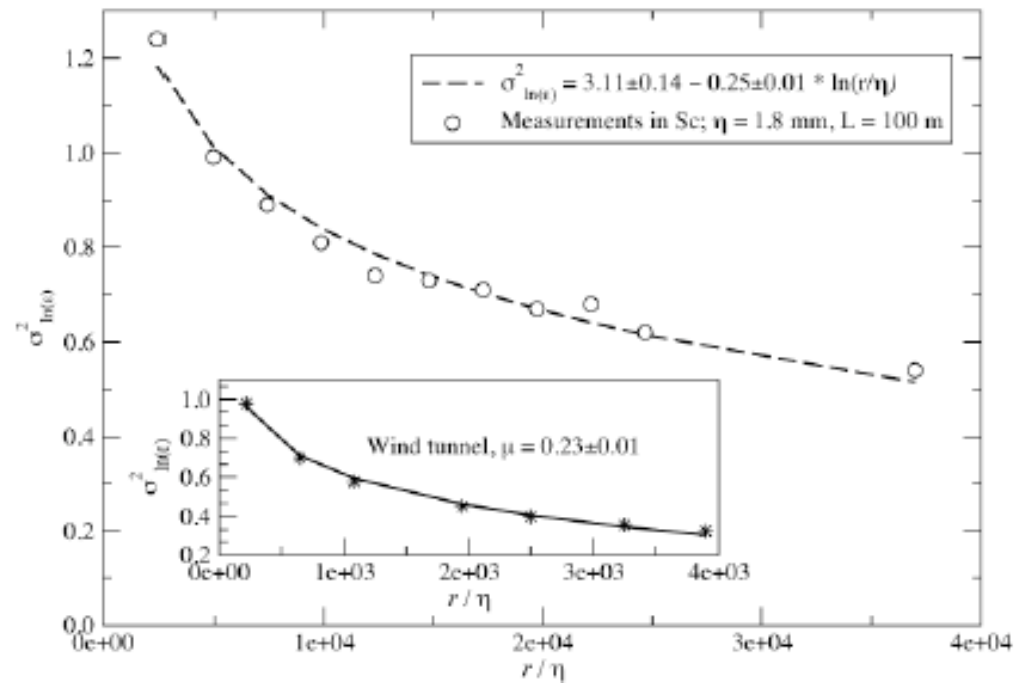
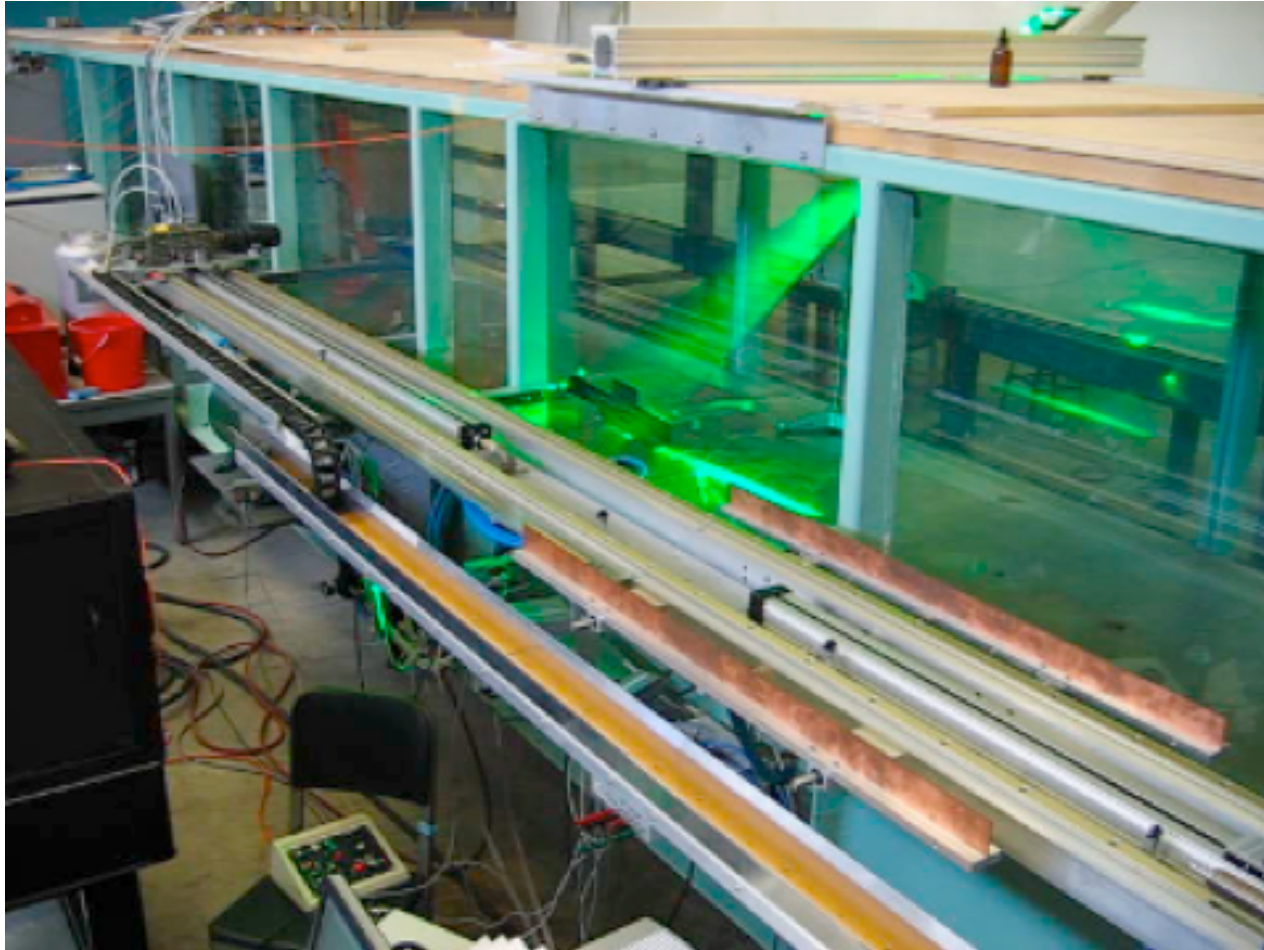


Figure 8: Variance $\sigma^2_{\ln(\epsilon_r)}$ as a function of the integration length r normalized with the Kolmogorov length $\eta \approx 1.8$ mm. An integral length scale $L \approx 100$ m limits $r/\eta < L/\eta \approx 5 \cdot 10^4$. A logarithmic fit (dashed line) yields an intermittency exponent $\mu = 0.25$ with a standard error of 0.01. Modified from Siebert et al. (2010).

Cornell Wind tunnel

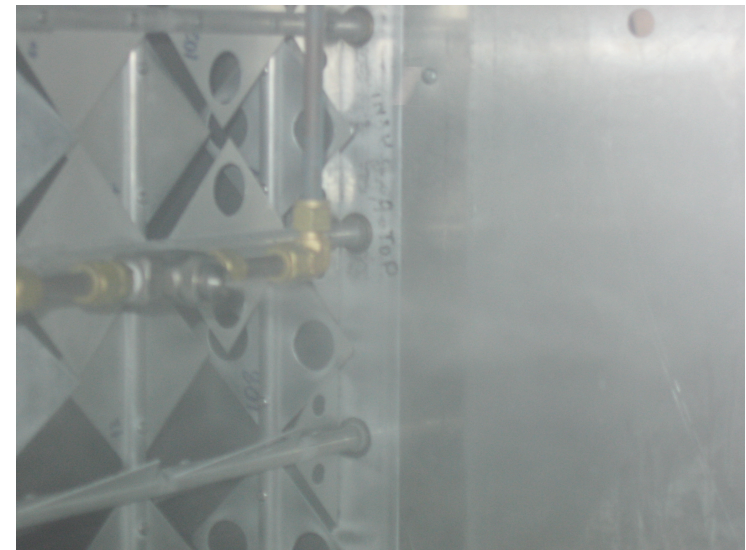


Spray System

- 4 air atomizing nozzles generate narrow distribution water droplets.
- Closed loop electro-pneumatic valves maintain accurate atomizing pressures.



- Spray injected directly behind turbulence generating grids.
- Mass loading can be varied between 10^{-4} - 10^{-3} (kg of water / kg of air)
- Number density 30 - 300 per cc for 20 μ m water droplets
- Particle size distribution log-normal.
- Distribution can be varied by changing atomizing air and water pressures



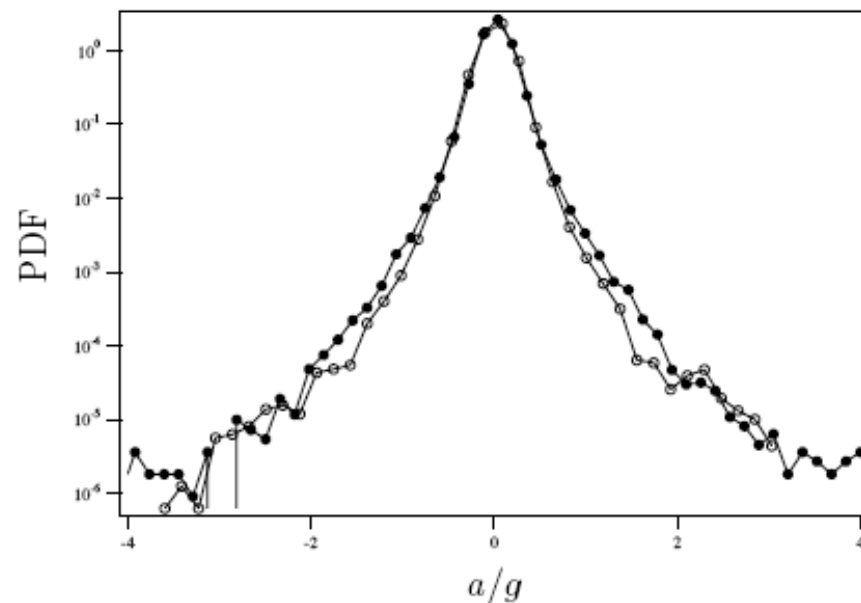
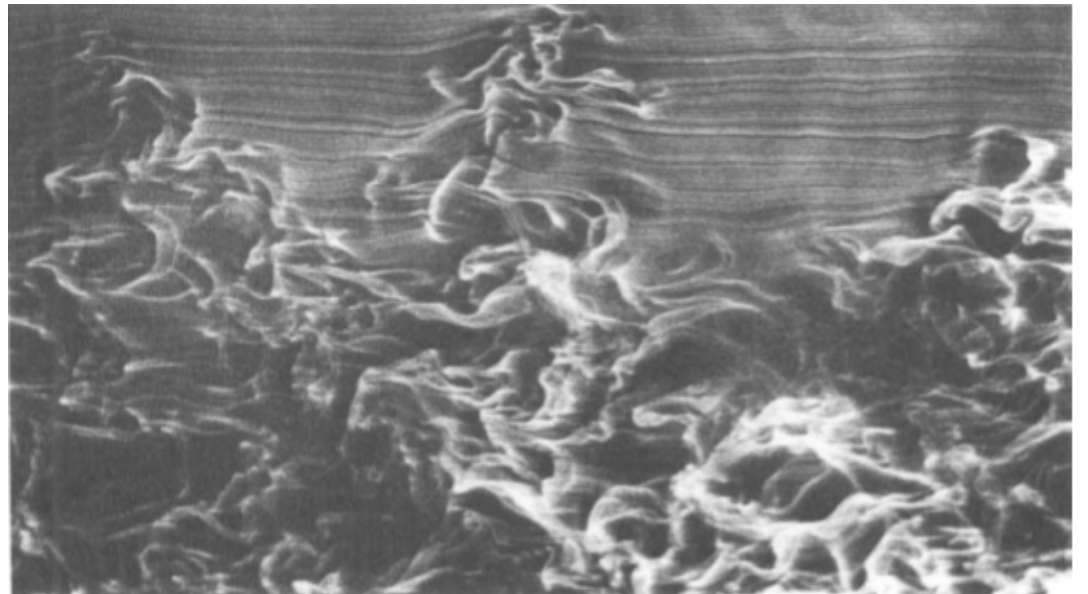


Figure 12: Probability density function of the Lagrangian acceleration of droplets in a turbulent wind-tunnel flow. The accelerations have been normalized by the gravitational acceleration and scaled to reflect atmospheric conditions (see text). The two PDFs are for flows with Taylor microscale Reynolds numbers $R_\lambda = 100$ (open circle) and 240 (filled circle) and Stokes number $St = 0.072$. Notice that the tails clearly show droplets undergoing accelerations greater than those due to gravity. Modified from Gerashchenko et al. (2008).

2. ENTRAINMENT



Jayesh & Warhaft, JFM,
277, 23, 1994



Entrainment

Very sharp interface with dry air, the relatively constant droplet size, and the existence of shear across the interface in some cases.

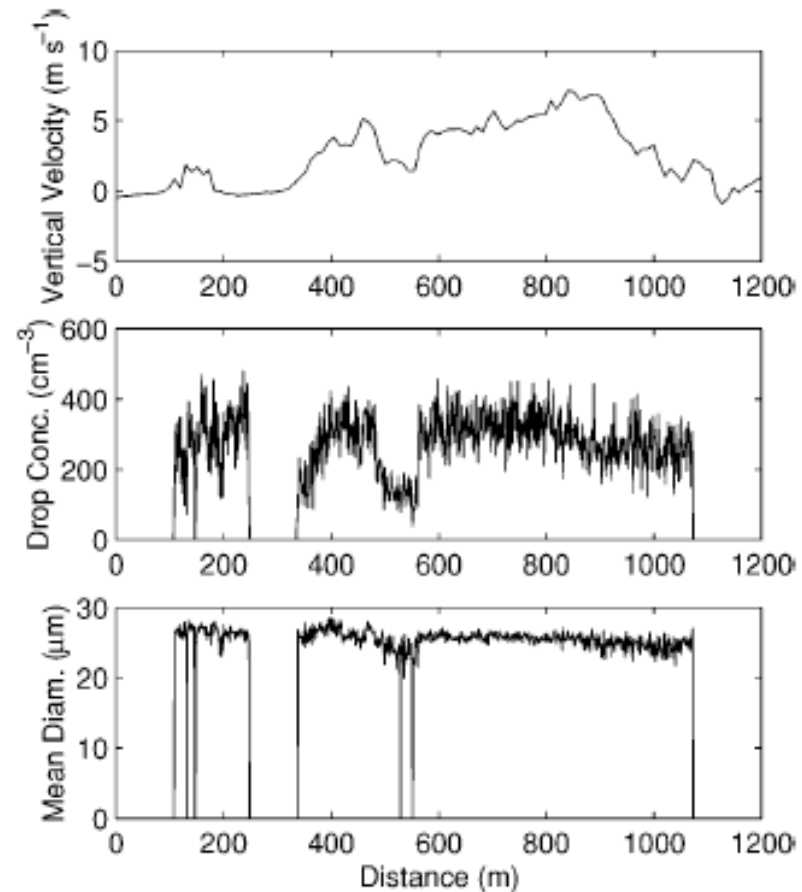
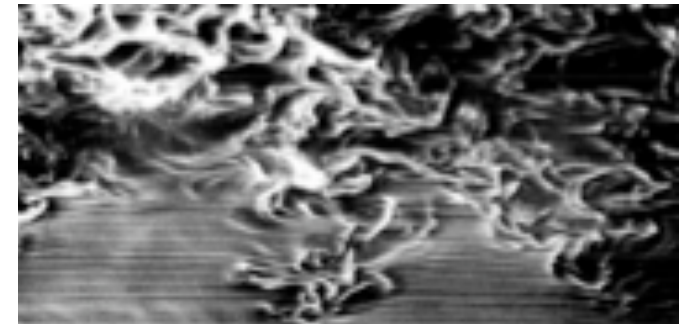


Figure 2 A traverse through a cumulus cloud. The top panel shows the vertical velocity, the middle panel shows droplet number density, and the bottom panel shows mean droplet radius. Note the sharp edges characteristic of the cloud-environment mixing process. Note also that to a large extent the mean radius fluctuates between a constant value and zero, implying that dry and cloudy air are largely segregated during much of the mixing process. Data from the SCMS field experiment, courtesy of J.-L. Brenguier, Météo-France.

Entrainment Experiment **with and without gravity** Sergiy Gerashchenko, Garrett Good, ZW

Shearless mixing layer (Veeravalli and W , 1989) .

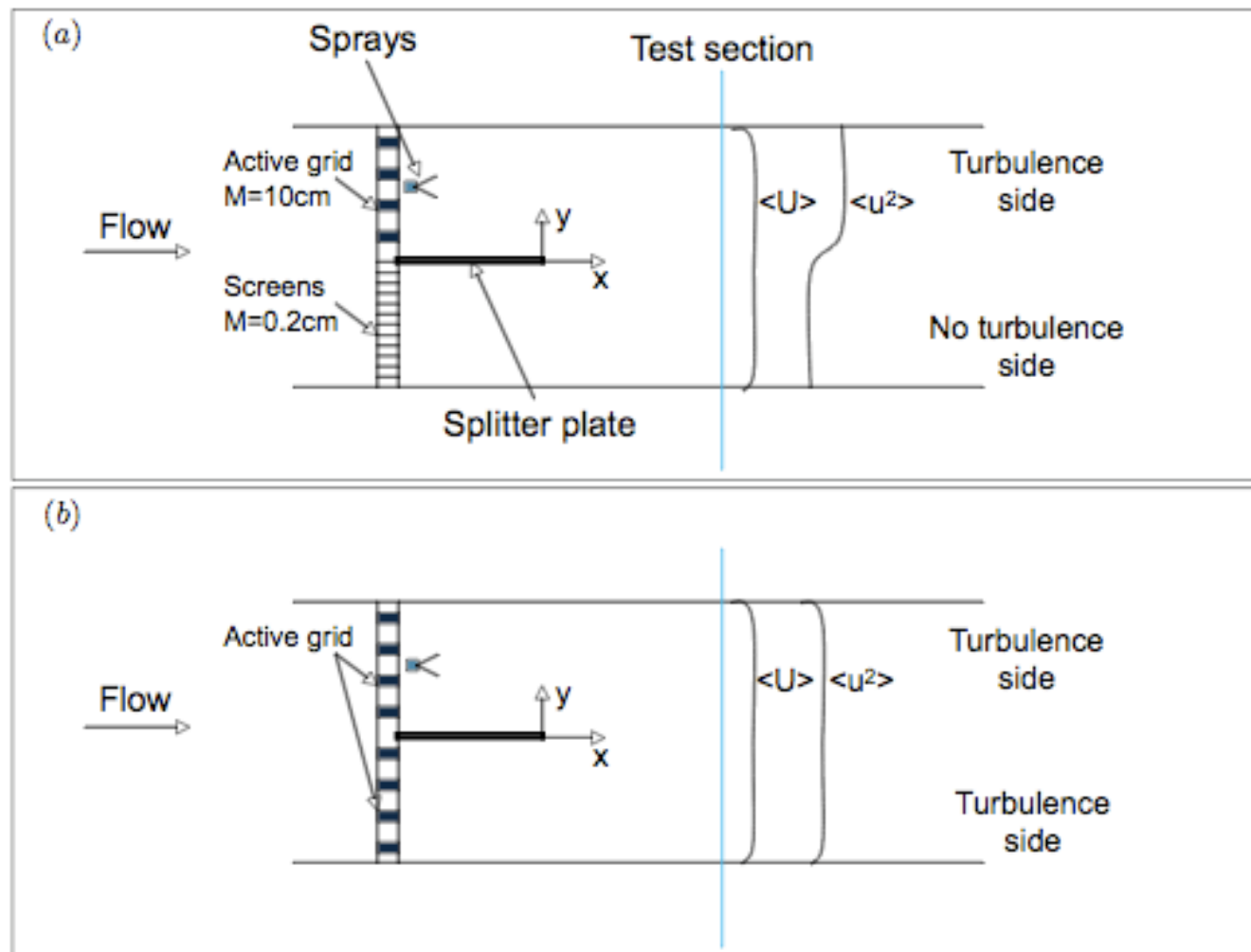


Turbulent non turbulent interface (TNI)

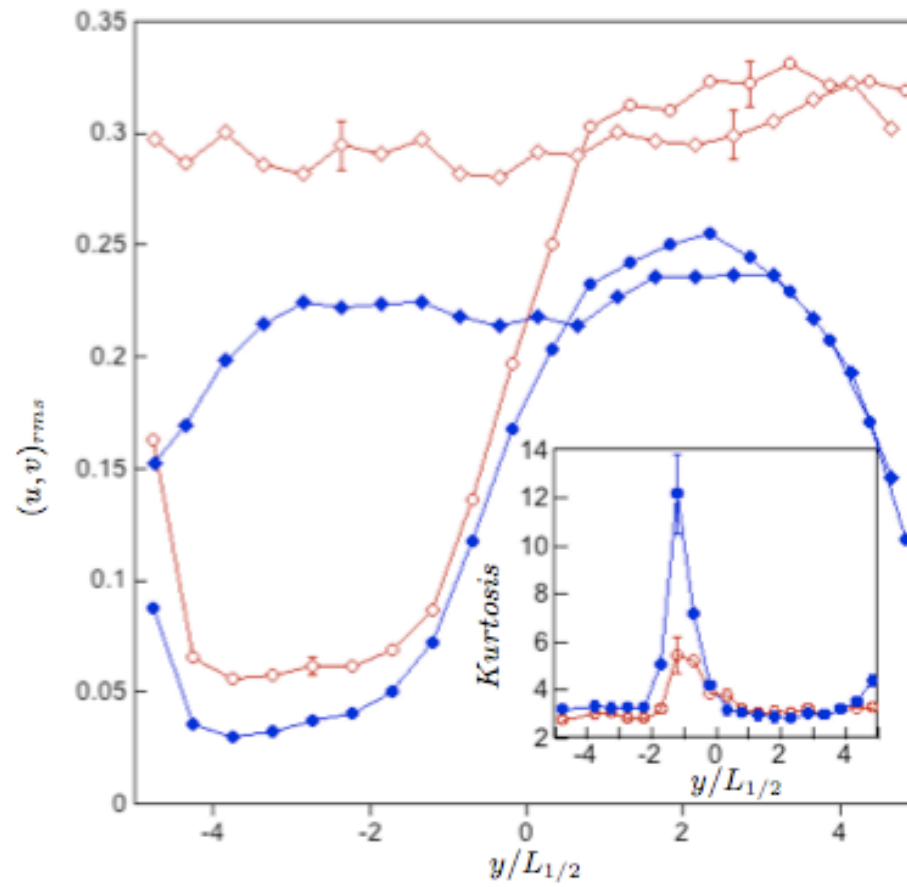
(No evaporation or collisions)

Also, Turbulence-turbulence interface (TTI)

Re_λ	$U(m/s)$	$u_{rms}(m/s)$	$v_{rms}(m/s)$	$TI(\%)$	$\epsilon(m^2/s^{-3})$	$\eta(mm)$
275(12)	2.15(0.05)	0.31(0.01)	0.24(0.01)	14.4(0.8)	0.138(0.006)	0.397(0.006)
$\tau_\eta(s)$	$\lambda(cm)$	$l(cm)$	St_η	St_l	Fr	
0.0105(0.0003)	1.3(0.04)	24(2)	0.2(0.03)	0.0028(0.0001)	0.54(0.01)	



S. Gerashchenko, G. Good, and Z. Warhaft

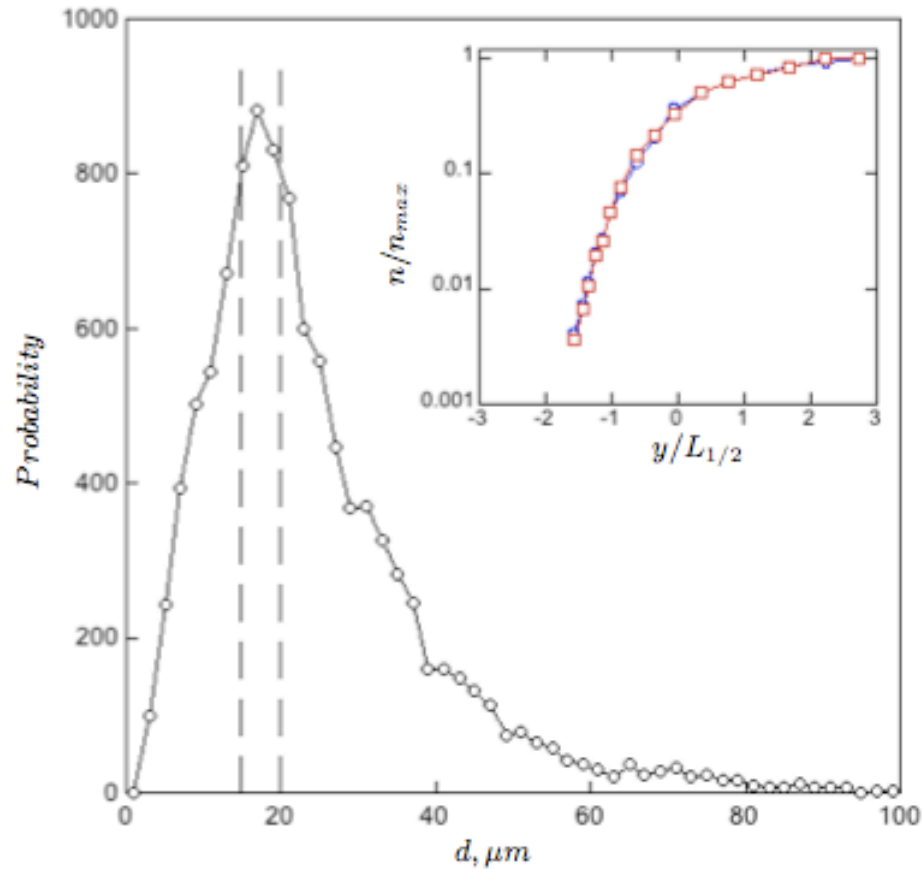


RMS velocity profiles and 4th moments: Hot wire measurements

Particle size distribution: Insert: Particles > 20 microns;
Partcles < 15 microns. **No difference Independent of St**

NO gravity case

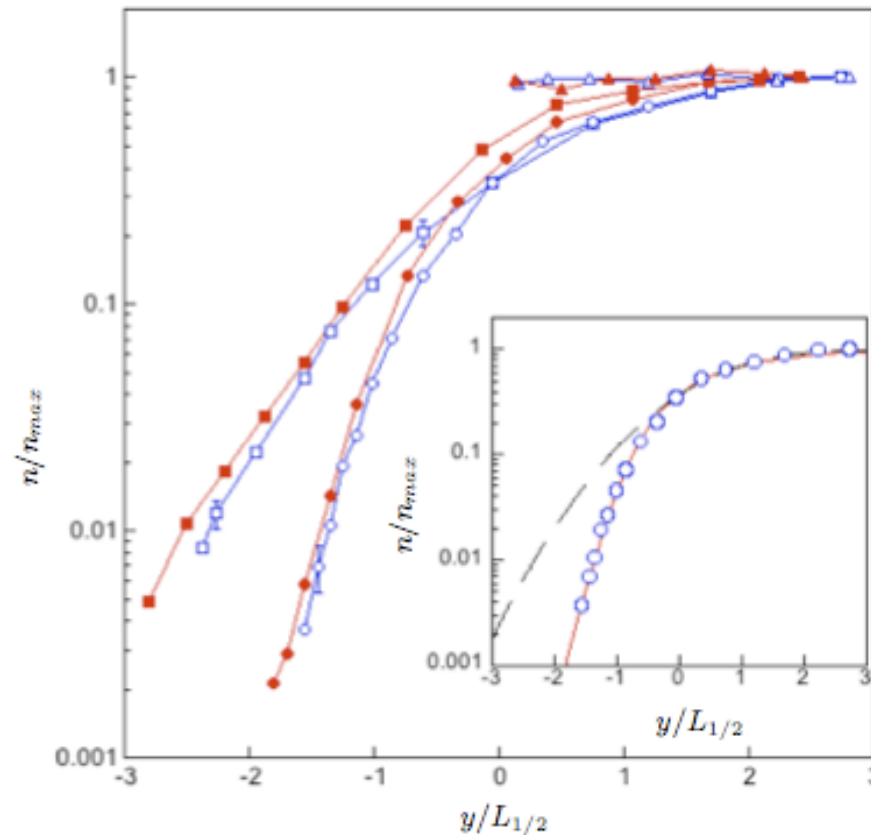
Geraschenko, Good &
Warhaft . 2010



Use St based on integral scale: $St_I \sim 0.003$

Concentration profiles TTI (squares) and TNI (circles): Red with g, blue no g.

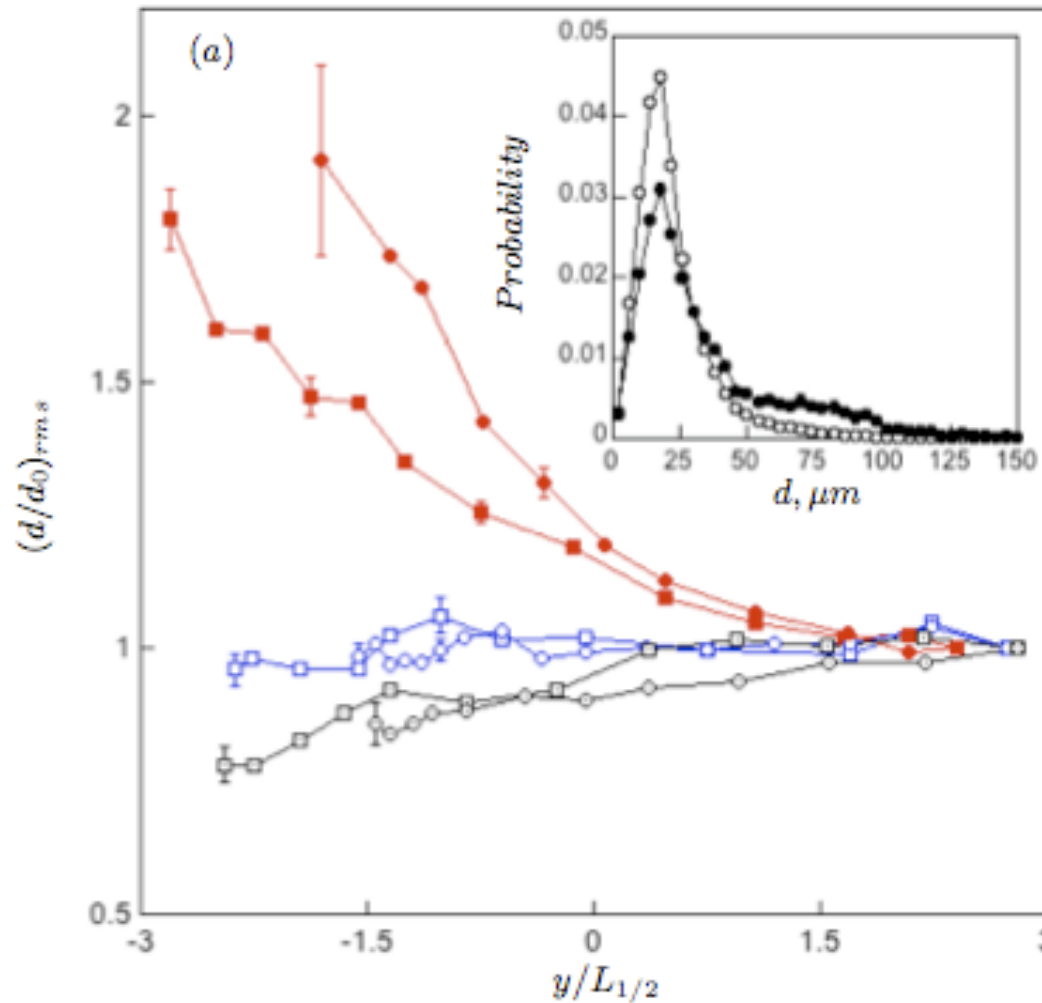
S. Gerashchenko, G. Good, and Z. Warhaft



Geraschenko,
Good &
Warhaft . 2010

Clearly TTI enhances mixing. Gravity accounted for in terms of Stokes flow

Particle diameter variation across layer: Red,
with g, blue no g, black negative g.

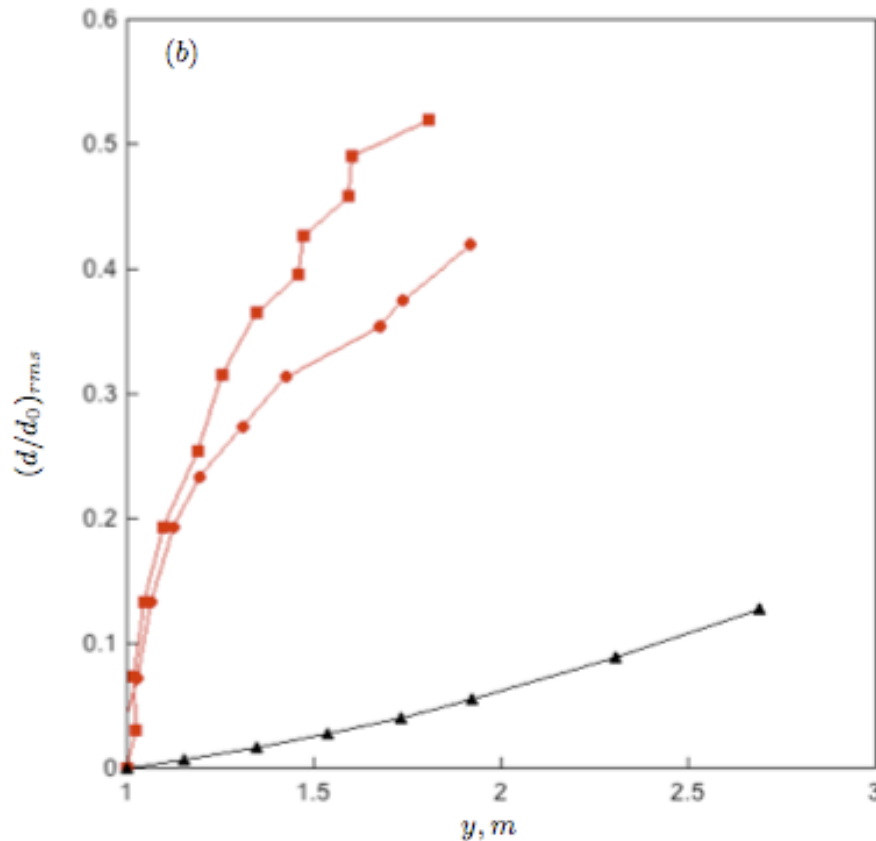


Circles TNI,
Squares,TTI

Geraschenko, Good &
Warhaft . 2010

Comparison with quiescent Stokes flow: Turbulence effects dominant in presence of gravity

(Maxey & Corrsin (1986), Davila & Hunt (2001), Aliseda et al (2002))



Geraschenko,
Good &
Warhaft . 2010

3. Boundary layer with and without gravity

QUESTION: How does shear affect the pdf's of inertial particles? The boundary layer experiments

Plan view

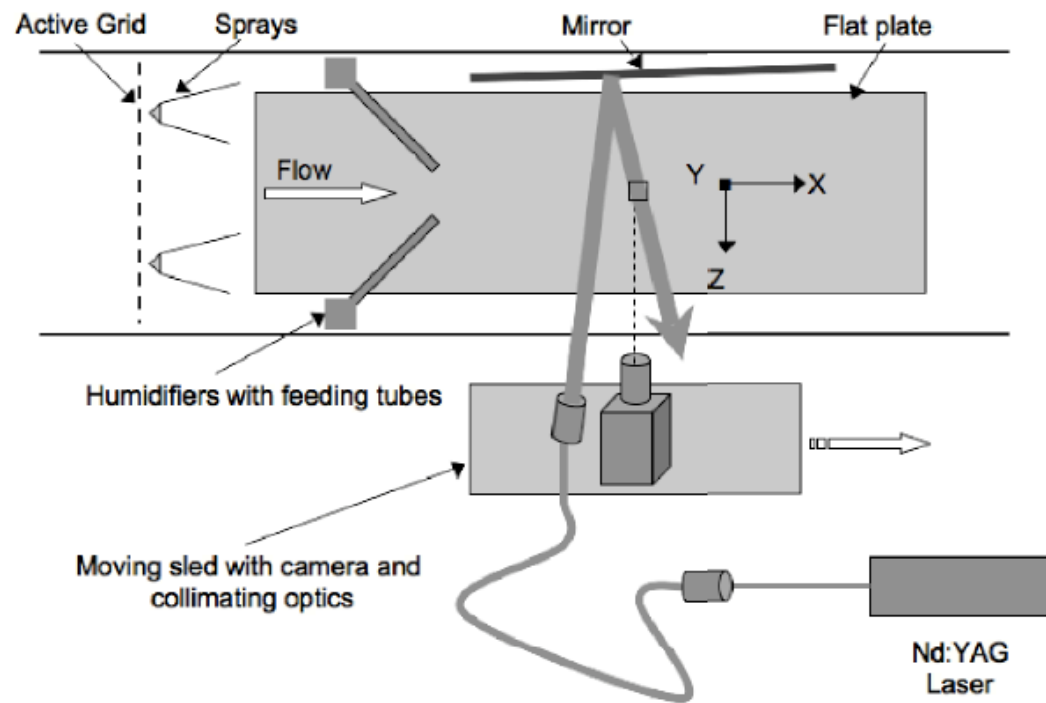


FIGURE 3. Schematic of the forward scatter experiment (top view). The two separate methods of introducing the droplets are shown together. When the sprays are operating, the humidifiers and feeding tubes are removed from the tunnel. The y coordinate is measured vertically from the plate.

Track characteristics--boundary layer

High speed Phantom v7.1 camera. Frame rate 8,000 fps, 512x512 pixels. Fiber optic cable attached to sled. Nd-YAG, 20W pulsed laser reflected from back mirror giving forward scatter at an angle of 5 degrees. 2mm. depth of focus.

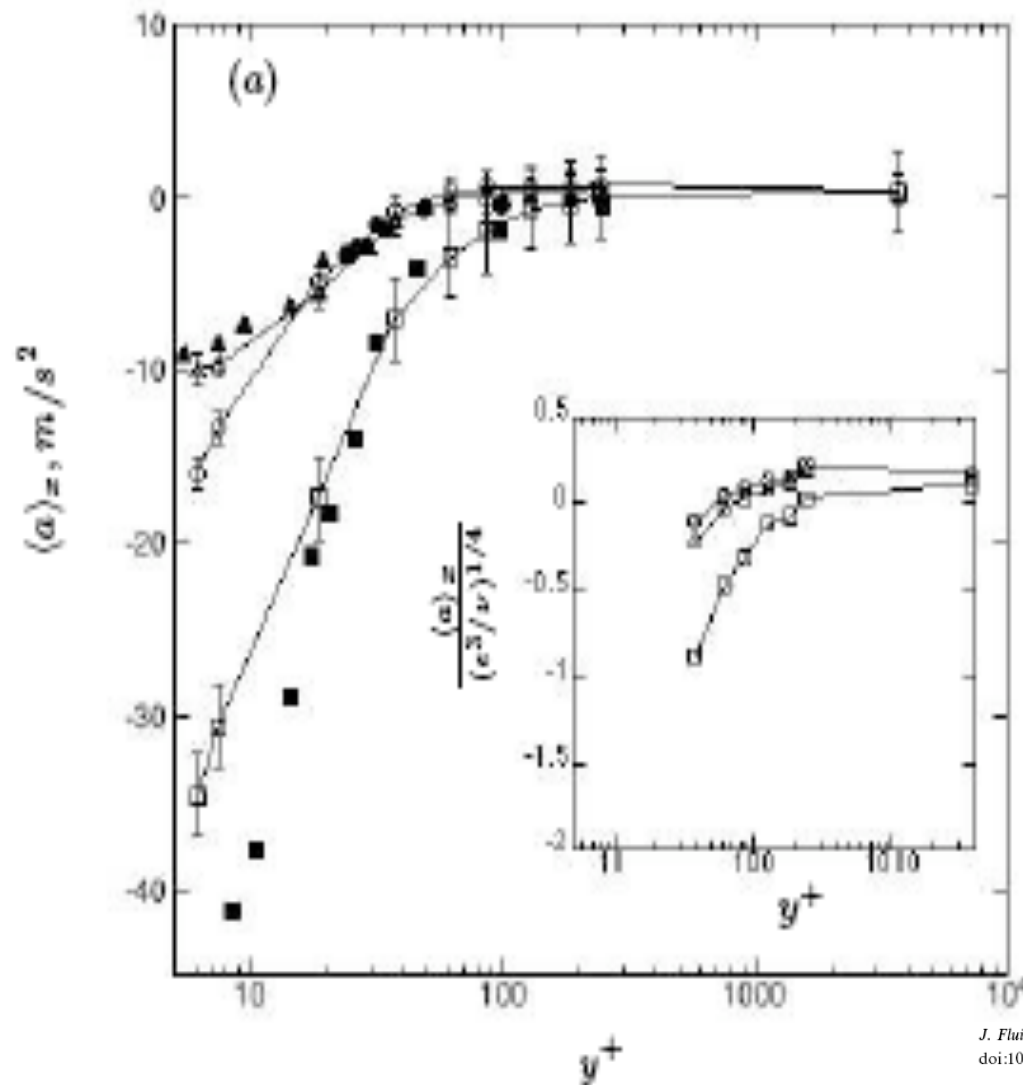
Particles tracked over distance of 50 cm. Sampling area 3.3x3.3 cm. Inter-sample time 0.0125 & 0.0042 Kolmogorov time units. Spatial resolution 0.148 & 0.097 Kolmogorov lengths.

1500 to 3000 sled runs providing 40 to 90 million acceleration estimates. Track length ~ 2 to 5 Kolmogorov lengths.

3.3 x 3.3 cm. field divided into strips and acceleration estimates were binned according to their locations.

Accelerations were calculated from measured particle tracks with Gaussian smoothing and differentiating filter (Voth et al. 2002).

The mean streamwise acceleration as a function of y^+



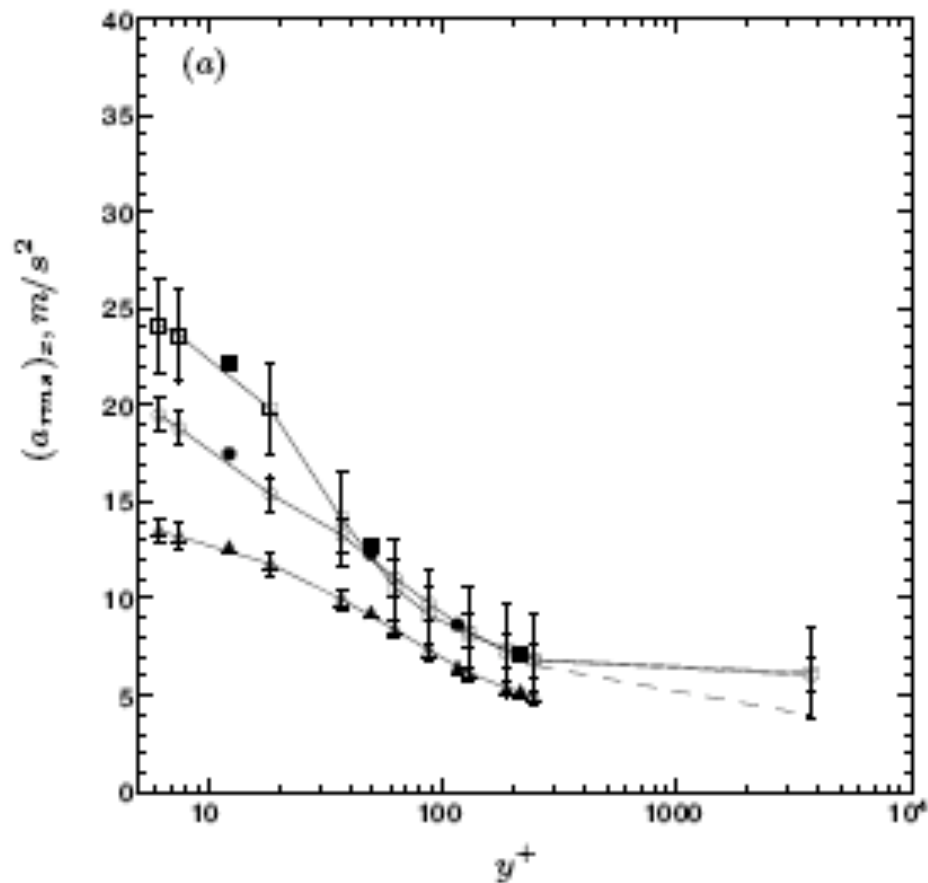
Squares: $St=0.47, Re=240$
 Circles: $St=0.07; St=240$
 Triangles: $St=0.035, Re=100$

Open symbols--experiment
 Filled symbols--model based
 on Maxey-Riley Equation.

Lagrangian measurements of inertial particle accelerations in a turbulent boundary layer

S. GERASHCHENKO, N. S. SHARP, S. NEUSCAMMAN
 AND Z. WARHAFT†

The rms acceleration as function of y^+



Squares: $St=0.47, Re=240$
Circles: $St=0.07; St=240$
Triangles: $St=0.035, Re=100$

Lagrangian measurements of inertial particle accelerations in a turbulent boundary layer

S. GERASHCHENKO, N. S. SHARP, S. NEUSCAMMAN
AND Z. WARHAFT†

On the role of gravity and shear on inertial particle accelerations in near-wall turbulence

JFM in press

V. LAVEZZO¹, A. SOLDATI¹
S. GERASHCHENKO², Z. WARHAFT²
AND L. R. COLLINS² †

6 *V. Lavezzo, A. Soldati, S. Gerashchenko, Z. Warhaft and L. R. Collins*

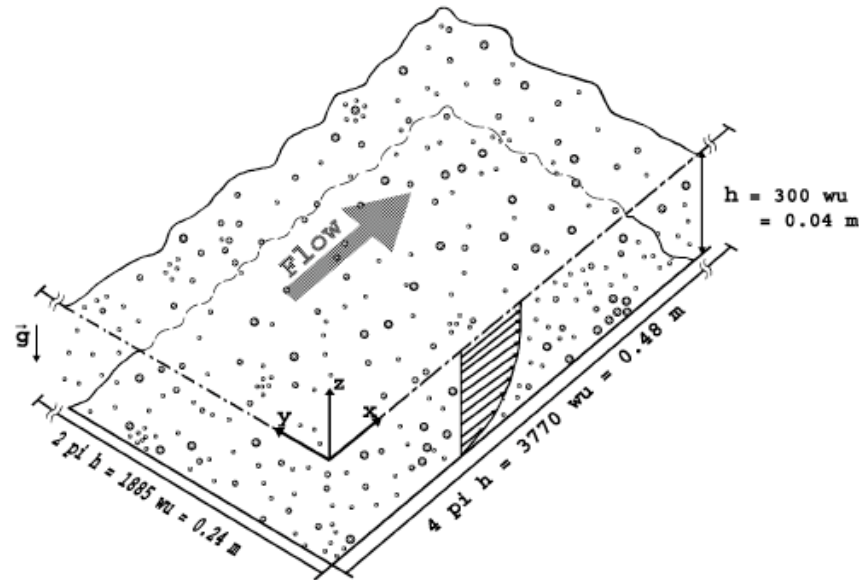


FIGURE 1. Lower half of the domain used in the channel flow DNS. Channel dimensions expressed in wall units (wu) are $4\pi h$ in the streamwise (x) direction, $2\pi h$ in the spanwise (y) and $2h$ in the wall-normal (z) direction with $h = 300$. A grid with $256 \times 256 \times 257$ points in the x , y and z direction respectively has been used to discretize the domain.

On the role of gravity and shear on inertial
particle accelerations in near-wall turbulence

V. LAVEZZO¹, A. SOLDATI¹
S. GERASHCHENKO², Z. WARHAFT²
AND L. R. COLLINS² †

Inertial particle accelerations in near-wall turbulence

9

	<i>Name</i>	u_τ [m/s]	<i>Height</i> [m]	Re_τ	g^+	d [μm]	St
	Low	0.112	$h = 0.04$	300	0.111	18.4	0.87
DNS	Med	0.112	$h = 0.04$	300	0.111	26.1	1.76
	High	0.112	$h = 0.04$	300	0.111	67.6	11.8

	Low	0.117	$\delta = 0.06$	470	0.091	16	0.72
Gerashchenko <i>et al.</i> (2008)	Med	0.124	$\delta = 0.1$	833	0.077	16	0.81
	High	0.124	$\delta = 0.1$	833	0.077	41	5.3

$$St \equiv \tau_p u_\tau^2 / \nu$$

On the role of gravity and shear on inertial particle accelerations in near-wall turbulence

V. LAVEZZO¹, A. SOLDATI¹
S. GERASHCHENKO², Z. WARHAFT²
AND L. R. COLLINS² †

JFM in press

Inertial particle accelerations in near-wall turbulence

19

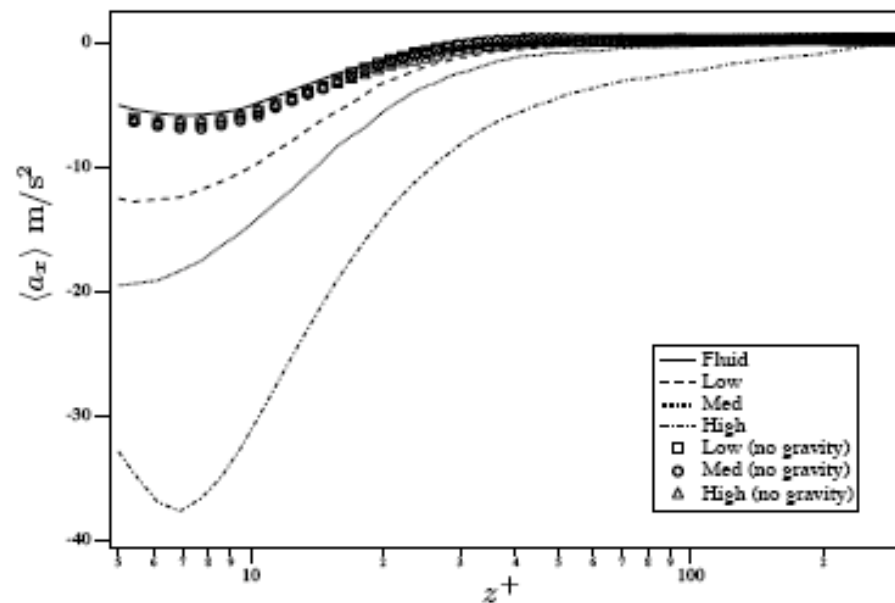


FIGURE 8. Mean particle acceleration in the streamwise direction at the three Stokes numbers, as indicated. Simulations results with gravity (lines) and without gravity (symbols).

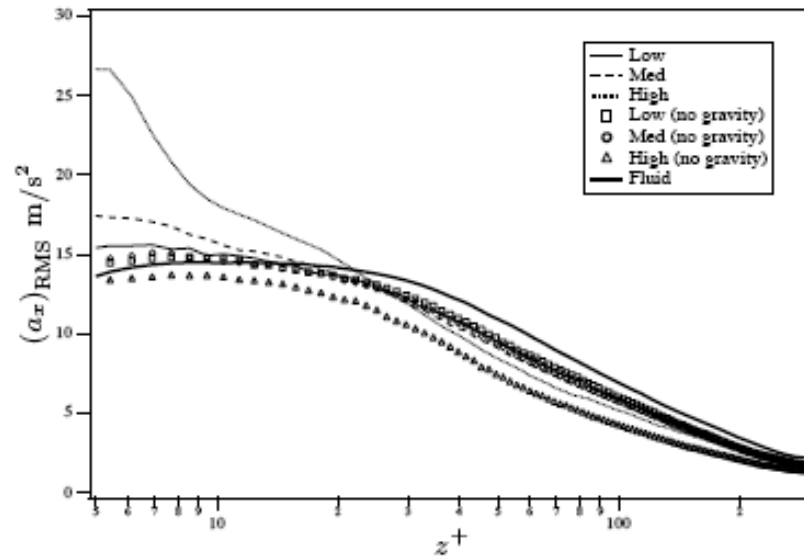


FIGURE 10. Effect of gravity on the RMS of particle acceleration fluctuations in the streamwise direction from the DNS. Simulation results with gravity (lines) and without gravity (symbols) are shown for the three Stokes numbers, as indicated.

Conclusions

Entrainment is strong function turbulence levels (obvious).

Concentration levels are slightly enhanced by gravity.

Size distribution is strongly affect by gravity.

Acceleration is strongly affected by gravity in the presence of shear

DNS confirms the importance of gravity in the case of shear
(for entrainment DNS is under way)

